Int. J. Electrochem. Sci., 17 **(2022)** Article Number: 22062, doi: 10.20964/2022.06.16

International Journal of
ELECTROCHEMICAL
SCIENCE
www.electrochemsci.org

Study of the Electrochemical and Electrical Properties $CoFe_2O_4$@GO/PEDOT Magnetic Nanocomposite for Microsupercapacitor Applications

Weiwei Wang[*], *Weike Zou*, *Qiubo Fan*

School of Physics and New Energy, Xuzhou University of Technology, Xuzhou, 221018, China
[*]E-mail: wwwang@xzit.edu.cn

Received: 2 December 2021 / *Accepted:* 6 January 2022 / *Published:* 7 May 2022

The structural, electrical, and electrochemical properties of $CoFe_2O_4$, graphene oxide and poly (3,4-ethylenedioxythiophene) ($CoFe_2O_4$@GO/PEDOT) as stretchable nanocomposite based microsupercapacitor (MSC) were characterized in this study. The hydrothermal method was used for the preparation of nanocomposite, and then designed into an array of 3×3 microelectrode by printing sacrificial patterns and pen lithography. XRD and FESEM studies demonstrated the successful synthesis of $CoFe_2O_4$@GO/PEDOT. Results of the electrical property of samples using 4-point probe method showed that the GO had the higher conductivity value, and electrical conductivity was decreased with the addition of $CoFe_2O_4$ and PEDOT to the GO based nanocomposite. Electrochemical studies using EIS, CV and GCD indicated good electrolyte ion diffusion on the $CoFe_2O_4$@GO/PEDOT surface and ideal capacitive behavior with fast redox reactions. The areal specific capacitance, energy density and power density of CoFe2O4@GO/PEDOT nanocomposites based MSCs were obtained at 435F/g, 62Wh/kg and 0.9W/kg, respectively, at a current density of 2.5A/g in electrolyte of 100g/l PVA/H_2SO_4. The comparison between the results for $CoFe_2O_4$@GO/PEDOT nanocomposite-based MSC and reported MSCs showed that the better or comparable performance than other reported MSCs can be attributed to the synergetic effect of the $CoFe_2O_4$@GO composite and porous conductive polymer PEDOT which provide good electrical conductivity and large surface area, indicating an improvement in the areal specific capacitance and energy density value and a decrease in power density. After 1000 cycles, the cycling stability of CoFe2O4@GO/PEDOT nanocomposite based MSCs showed an amazing capacitance retention of about 96%, exhibiting good cycling stability of $CoFe_2O_4$@GO/PEDOT nanocomposite based MSCs.

Keywords: Microsupercapacitor; Gel electrolyte; Graphene magnetic nanocomposite; Electrical properties; Areal specific capacitance

1. INTRODUCTION

Today, the development and application of stretchable microscale electronics to miniaturize industrial, medical and energy harvesting devices such as cameras, mobile and personal entertainment

devices, calculators, exercise monitors, and wearable electronics such as electronic skins and healthcare monitoring systems causes significant competition in the market [1, 2]. More importantly, MSCs as flexible energy storage tools on-chip microscale devices have grown in popularity, and numerous studies have been conducted to discover suitable materials and electrode configurations in the development of MSC technology [3-6].

Accordingly, research has shown that most MSCs show good performance *in wave-like*, honeycomb kirigami, bridge-island, cellular, helical and textile fiber electrodes configurations [7-9]. Many studies have been conducted on, MnO_2RuO_2, Ag@Ppy, V_2O_5, VS_2, MXene, PEDOT: PSS, porous carbon, graphene, and MWCNTs-based electrochemical [10-12]. Even so, application of the stretchable MSCs is faced with challenges due to poor mechanical stability and weak cycling and rate performance [13, 14]. Moreover, the manufacturing process of *MSCs* is also highly sensitive, and not only requires complicated and multistep processing involving expensive equipment but also need to work in a clean room [15-17].

As a result of the large market and increasing demand for MSCs, ongoing research is being conducted to overcome problems in design and development of fabrication methods with favorable materials to improve the capacity and stability of MSCs [18-20]. Therefore, this study presented the fabrication of $CoFe_2O_4$@GO/PEDOT as a graphene based magnetic nanocomposite and the study of its structural and electrical properties and electrochemical characterizations for MSC applications.

2. EXPERIMENTAL

2.1. Synthesis of $CoFe_2O_4$@GO/PEDOT

The hydrothermal method was used for the preparation of a mixture of $CoFe_2O_4$@GO [21]. GO (>95wt%, Xiamen Tob New Energy Technology Co., Ltd., China), $Fe(NO_3)_3 \cdot 9H_2O$ (99%, Merck, Germany) aqueous solution, and $Co(NO_3)_2 \cdot 6H_2O$ (99%, Merck, Germany) aqueous solution were mixed in a molar ratio of 3:2:1 using magnetic stirring for 12 minutes. Then, the mixture was transferred to a Teflon-coated stainless steel autoclave and heated at 130°C for 12 hours. After cooling, the obtained black product was washed with ethanol three times, and dried at 55°C in the oven. 2g of The $CoFe_2O_4$@GO was ultrasonically added in 10 mL of n-butyl acetate (≥99.5%, Sigma-Alderich) containing 50 µl/ml of poly(3,4-ethylenedioxythiophene) (PEDOT, 97%, Sigma-Alderich) to obtain the homogeneous nanocomposite ($CoFe_2O_4$@GO/PEDOT).

2.2. Preparation of microsupercapacitors of $CoFe_2O_4$*@GO/PEDOT*

For the preparation of an array of 3 × 3 microsupercapacitors (MSC), a pattern electrode was designed by printing sacrificial patterns using a commercial laser printer (DIY 2500w, Shenzhen Twotrees Technology Co., Ltd., China). The magnetic nanocomposite-based MSC was successfully fabricated on a transparent commercial polyethylene terephthalate (PET, Taizhou Shantai Packaging Co., China) film. Subsequently, the magnetic nanocomposite ink was loaded onto the substrate using a rollerball pen. Following that, 1 ml of 0.7 g/ml $Fe(ClO_4)_3$ (99%, Sigma-Alderich) solution was

dropped directly onto the magnetic nanocomposite electrode and allowed to polymerize for 60 minutes at room temperature [22]. The resulted array was washed with absolute ethanol (99%, Shandong Baovi Energy Technology Co. Ltd., China) and deionized (DI) water thoroughly and then dried at room temperature for 40 minutes. The sample was carefully washed sequentially with acetone (99.5%, Shandong Baovi Energy Technology Co. Ltd., China) and DI water to remove the unwanted printer pattern and template from the substrate.

2.3. Fabrication of a GO/PEDOT nanocomposite-based MSC with a flexible microelectrode

The GO/PEDOT ink was synthesized by a mixture of GO, n-butyl acetate and 50μl/ml PEDOT in a volume ratio of 2:1:1. The mixture was sonicated for 60 minutes to achieve a homogeneous suspension [22], followed by the deposition of GO/PEDOT. For polymerization, 0.7 g/ml of $Fe(ClO_4)_3$ solution was slowly dropped on the GO/PEDOT electrode. After 60 minutes, the GO/PEDOT electrode was washed with a mixture of ethanol and DI water, and then dried at room temperature for 40 minutes. Afterwards, the silicone rubber coating (Aerol Formulations P. Ltd., India) was applied for the rubber coating of the surface of the GO/PEDOT electrode.

In order to assemble the flexible MSC, silver paste (Zhongshan Maxtor New Material Co., Ltd., China) was employed to meticulously connect each MSC to the GO/PEDOT electrode structure. Afterwards, the gel electrolyte was prepared by adding 2 g of polyvinyl alcohol (PVA, 99%, Jinzhou City Yicheng Cellulose Co., Ltd., China) into 2 g of H_2SO_4 (99.99%, Sigma-Alderich) and 20 ml of DI water. The electrolyte was stirred at 85°C to obtain the transparent solution that it was spread onto the MSC arrays. The MSCs were dried at room temperature for 10 hours.

2. 4. Structural and electrical characterizations

Field emission scanning electron microscopy (FESEM, SU8010, Hitachi Co., Tokyo, Japan) was used to study the morphological properties of nanocomposite. For crystal structure analysis, X-ray diffraction (XRD, Bruker Nanostar U) with Cu Kα radiation (λ = 0.1542 nm) at 45 kV was applied. In order to study the electrical properties, electrical conductivity measurements were carried out using a pellet (Φ20 mm × 0.5 mm) prepared from the synthesized nanocomposites with a pressure of 20 MPa, and 4- point probe method (ST2558B-F01, Suzhou Jingge Electronics Co., Ltd.,China) was employed for the electrical conductivity of pressed pellets at room temperature under an applied current of 10 mA. Four electrical contacts were arranged in a line with uniform pin separation (1.5 mm) and placed on the surface of the sample.

2.5. Electrochemical studies

The electrochemical analyses of MSC arrays including cyclic voltammetry (CV), electrochemical impedance spectroscopy (EIS) and galvanostatic charge-discharge (GCD) were carried out in a potentiostat/galvanostat electrochemical workstation (Corrtest, Wuhan Corrtest Instruments Corp., Ltd., China) using both three-electrode and two-electrode systems. In the three-

electrode system, a prepared single microelectrode is used as a working electrode, a Pt wire as counter and a saturated calomel electrode (SCE) as a reference electrode. In the two-electrode system, two electrodes are employed as the working and the counter electrodes, respectively. An EIS was employed for a frequency range from 10^5 Hz to 10^{-2} Hz and sinusoidal amplitude of 10 mV. EIS data was fitted based on an equivalent electrical circuit model using ZSimpWin software. The areal specific capacitance (C_s) was calculated by the equation (1) [23, 24]:

$$C_s = I\Delta t/S\Delta V \quad (1)$$

Where I and Δt are the constant discharge current and the discharge time, respectively. ΔV is the applied potential interval, and S is the electrode area. The energy density (E) and power density (P) were calculated according to the following equations (2) and (3), respectively [25, 26]:

$$E = C \times (\Delta V)^2/7200 \quad (2)$$

$$P = E \times 3600/\Delta t \quad (3)$$

3. RESULTS AND DISCUSSION

3.1. Structural characterization

Figure 1 illustrates the XRD patterns of powders of GO nanosheets, $CoFe_2O_4$, $CoFe_2O_4$@GO and $CoFe_2O_4$@GO/PEDOT. The XRD pattern of powders of GO shows a sharp diffraction peak at 2θ = 10.04°, which is related to the (001) plane [27]. The XRD pattern of $CoFe_2O_4$ shows the diffraction peaks at 2θ = 18.27°, 30.21°, 35.56°,37.34°, 43.14°, 53.69°, 56.98°, 62.72° and 74.28°, corresponding to the (111), (220), (311), (222), (400), (422), (511), (440) and (533) planes, respectively, which represent to crystal phase of $CoFe_2O_4$ with a spinel structure based on JCPDS card No. 00-022-108 [28, 29]. The XRD pattern of $CoFe_2O_4$@GO exhibits all diffraction peaks of $CoFe_2O_4$ and GOES, indicating the successful synthesis of $CoFe_2O_4$@GO nancomposite. Moreover, the XRD pattern of the $CoFe_2O_4$@GO/PEDOT shows all the diffraction peaks of $CoFe_2O_4$@GO nancomposite and an additional low intensity at 2θ=26.18° which is related to the intermolecular spacing of the polymer backbone that is assigned to the (020) reflection [30], demonstrating the successful synthesis of $CoFe_2O_4$@GO/PEDOT.

Figure 2 presents the FESEM images of GO, $CoFe_2O_4$, $CoFe_2O_4$@GO and $CoFe_2O_4$@GO/PEDOT. The FESEM image of GO in Figure 2a reveals agglomerated micro-sized nanosheets with an average thickness of 10nm. As observed from Figure 2b, $CoFe_2O_4$@GO/PEDOT shows the presence of $CoFe_2O_4$ nanoparticles that are distributed on GO nanosheets and the coral-like morphology of PEDOT. Conjugated -bonds are present in the PEDOT structure, and interactions between the PEDOT molecule and GO nanosheets can be strong due to - stacking and the van der Waals force [31-33]. It can be seen that the polymerized nanocomposite ink of $CoFe_2O_4$@GO/PEDOT provide the high porosity surface. Furthermore, $CoFe_2O_4$ nanoparticles have a synergistic effect on increasing effective surface area by reducing π-π interactions between sheets [34, 35], and the

electrostatic repulsion between the negatively charged $CoFe_2O_4$@GO/PEDOT [36, 37]. In addition, the bonding of PEDOT with GO nanosheets enhances the surface roughness.

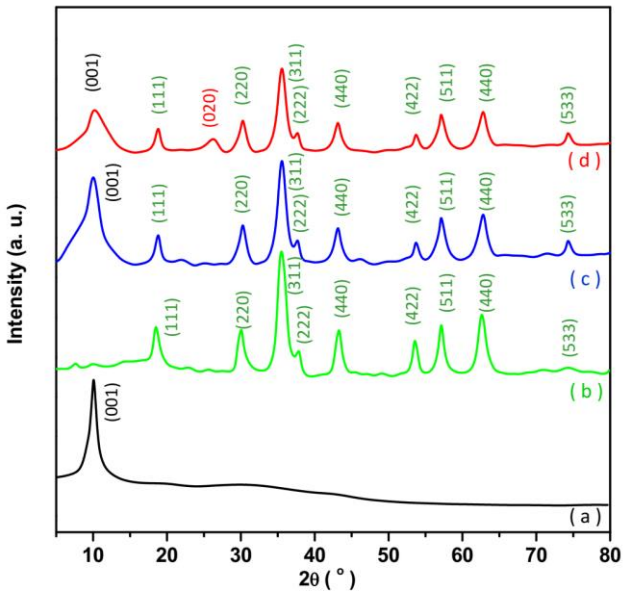

Figure 1. XRD patterns of powders of (a) GO nanosheets, (b) $CoFe_2O_4$, (b) $CoFe_2O_4$@GO and (d) $CoFe_2O_4$@GO/PEDOT.

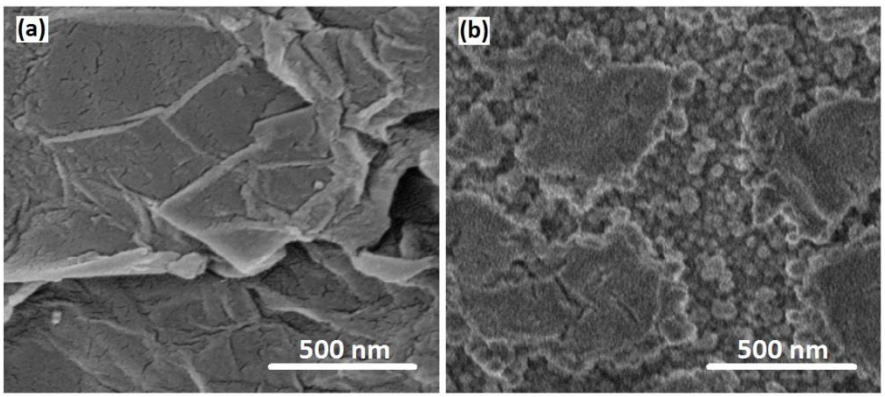

Figure 2. FESEM images of (a) GO, (b) $CoFe_2O_4$, (b) $CoFe_2O_4$@GO and (d) $CoFe_2O_4$@GO/PEDOT

3.2. Electrical characterizations

Table 1 presents the conductivity (σ) and resistivity (ρ) values of synthesized d GO, $CoFe_2O_4$, $CoFe_2O_4$@GO and $CoFe_2O_4$@GO/PEDOT nanocomposites. As observed from Table 1, the GO has the higher conductivity value, and electrical conductivity is decreased with the addition of the $CoFe_2O_4$ and PEDOT to the GO-based nanocopmposite. $CoFe_2O_4$ also shows lower conductivity. The variation in electrical conductivity can be described in terms of percolation theory [38, 39]. Based on this theory,

the remarkable increase in conductivity occurs when the concentration of conductive filler exceeds its critical value. In composites containing conducting (ρ) and semiconducting (ρ_c) components, the relation between the electrical conductivity of the conducting-superconducting mixture of the percolation threshold is described by a simple power law $\sigma \sim (\rho-\rho_c)^t$, where the critical exponent t depends only on the dimensionality of the system [40, 41].

3.3. Electrochemical characterizations

EIS measurement was used to characterize the interface quality between the electrode and electrolyte, and study the capacitive and resistive behavior of samples. Generally, the Nyquist plot consists of three components: (i) a high-frequency intercept on the real Z'axis which mainly concerns the contribution of the electrolyte resistance, the intrinsic resistance of the active electrode material, and the contact resistance at the interface, (ii) a semicircle in the high-to-medium-frequency region which corresponds to the charge transfer reaction at the interface between the electrode and the electrolyte, and (iii) a straight line at the very low-frequency region associated with electrolyte ion diffusion [42]. Figure 3a exhibits the Nyquist plots for all samples in the frequency range from 10^5Hz to 10^{-2}Hz with sinusoidal amplitude of 10 mV. As seen, there are no semicircles at the mid-frequency region for all the electrodes, implying to the possibility of electrochemical reactions related to the redox conversion of Fe^{3+}/Fe^{2+} [43]. All samples show an EIS curve which is composed of a short arc and diagonal line with a slope of 45 (Warburg line), demonstrating good electrochemical capacitive behavior [44, 45]. Figure 3c depicts the resulting equivalent electrical circuit based on EIS data analyses, which includes series resistance (Rs), Warburg resistance (ZW), and capacitance (CPE) [46]. The obtained parameters are shown in Table 1 which indicates the lowest Rs belonged to the $CoFe_2O_4$@GO/PEDOT sample.

Figure 3b depicts the CV curves of GO, $CoFe_2O_4$@GO, $CoFe_2O_4$/PEDOT and $CoFe_2O_4$@GO/PEDOT nanocomposite based MSCs at a scan rate of 20mV/s. As seen in the CV curves of $CoFe_2O_4$@GO, $CoFe_2O_4$/PEDOT and $CoFe_2O_4$@GO/PEDOT, there are two pairs of redox peaks that result from the electrochemical reaction of the redox-active couples in the electrolyte: $Fe^{3+} + e^- \leftrightarrow Fe^{2+}$ [47]. The specific capacitance is proportional to the integral area of the CV curves as following equation [48-50]:

$$i_p = (2.687 \times 10^5)\, n^{3/2} A\, C\, D^{1/2}\, \nu^{1/2}\, C \qquad (1)$$

Where i_p is the peak current and n corresponds to the count of transferred electrons. A represents the electrochemical active surface area (cm^2), D is diffusion co-efficient, and υ and C denote the scan rate (V/s) and analytic amount, respectively. As seen, the surrounded area in the CV curve in $CoFe_2O_4$@GO/PEDOT in larger than GO and $CoFe_2O_4$@GO. Thus, the large specific capacitance of $CoFe_2O_4$@GO/PEDOT is derived from the $CoFe_2O$ phase instead of GO and PEDOT which may be related to the large availability of active sites of $CoFe_2O_4$ nanoparticles that decorated GO nanosheets and coral-like morphology of PEDOT [51], and synergistic effect in improving the electrical conductivity in $CoFe_2O_4$@GO/PEDOT by mixing high conductive PEDOT and GO nanosheets [52].

Furthermore, the CV curves of $CoFe_2O_4$@GO/PEDOT are almost rectangular, which is associated with ideal capacitive behavior with fast redox reactions [53, 54].

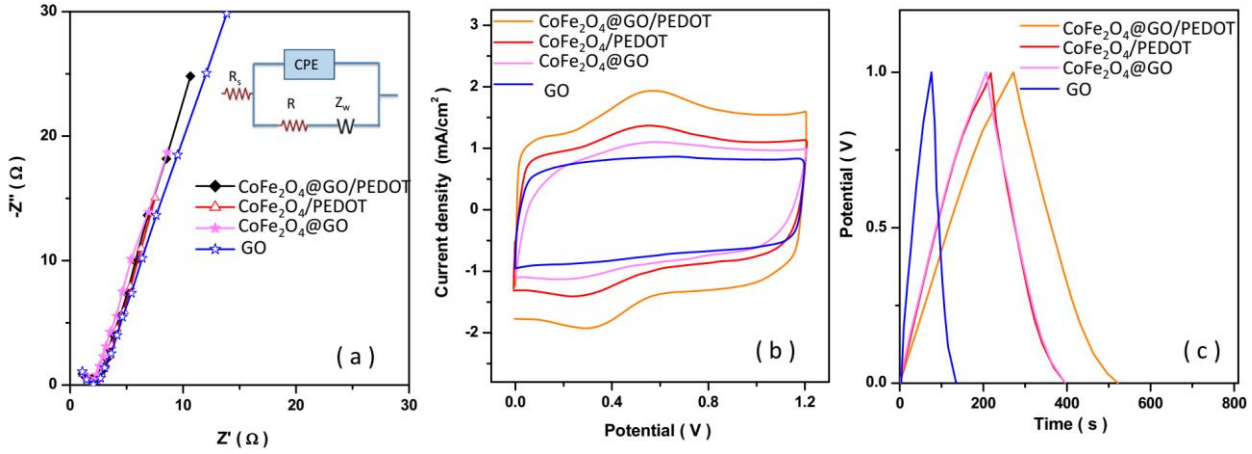

Figure 3. (a) Nyquist plots at 10 mV potential, (b) CV at 20 mV/s scan rate, (c) GCD curves at 2.5 A/g current density in potential range from 0 to 1.2 V for GO, $CoFe_2O_4$@GO, $CoFe_2O_4$/PEDOT and $CoFe_2O_4$@GO/PEDOT.

Table 1. The obtained values for C_s, E and P of GO, $CoFe_2O_4$@GO, $CoFe_2O_4$/PEDOT and $CoFe_2O_4$@GO/PEDOT nanocomposites based MSCs.

Sample	**Rs (Ω)**	**Z_W (Ω/S)**	**CPE (F)**	**σ (S/m)**	**ρ(Ω m)**
GO	1.31	0.049	0.025	18.33	5.44×10^{-2}
$CoFe_2O_4$@GO	1.29	0.144	0.085	15.80	6.61×10^{-2}
$CoFe_2O_4$/PEDOT	1.42	0.095	0.071	5.25	1.91×10^{-1}
$CoFe_2O_4$@GO/PEDOT	1.05	0.150	0.116	13.97	7.18×10^{-2}

Figure 3c displays the GCD curves of GO, $CoFe_2O_4$@GO, $CoFe_2O_4$/PEDOT and $CoFe_2O_4$@GO/PEDOT nanocomposites based MSCs obtained at a current density of 2.5 A/g. It can be observed that oFe_2O_4/PEDOT and $CoFe_2O_4$@GO/PEDOT nanocomposites show a symmetric, triangle-shaped charge discharge profile in the GCD curve, implying good reversibility. There is a considerable enhancement in the charge storage capacity of $CoFe_2O_4$@GO/PEDOT nanocomposite based MSCs as compared to the other MSCs, and they also show significantly longer charging/discharging time as compared to other MSCs. The overwhelming long charge/discharge times are related to the pseduocapactive characteristics of the $CoFe_2O_4$@GO/PEDOT electrode and the good charge storage property of the PEDOT in the energy storage systems [55-57]. The obtained values for C_s, E and P of GO, $CoFe_2O_4$@GO, $CoFe_2O_4$/PEDOT and $CoFe_2O_4$@GO/PEDOT nanocomposites based MSCs are presented in Table 2. It can be found that the synergistic effect of the GO and $CoFe_2O_4$ in the PEDOT matrix resulted in an improvement of the areal specific capacitance and energy density value and a decrease in the power density.

The increase in the capacitance in the $CoFe_2O_4$@GO/PEDOT electrode is can be related to the change in the nanostructures, the high porosity between the $CoFe_2O_4$ nanoparticles, GO nanosheets with numerous edges and coral-like morphology of the PEDOT matrix can facilitate the penetration and movement of electrolyte ions into the inner region of the electrode. The resultant large surface area of the $CoFe_2O_4$@GO/PEDOT nanocomposite gives more active sites for electrochemical reactions and enhances the charge transfer rate to the $CoFe_2O_4$@GO/PEDOT [58-60]. PEDOT combined with GO nanosheets enhances the conductivity at reducing potentials, indicting better electrochemical performance of MSCs due to their good chemical and physical stability, wide tenability composition, and electrolyte compatibility [31]. Therefore, further electrochemical studies were conducted on the $CoFe_2O_4$@GO/PEDOT electrode.

Table 2. The obtained values for C_s, E and P of GO, $CoFe_2O_4$@GO, $CoFe_2O_4$/PEDOT and $CoFe_2O_4$@GO/PEDOT nanocomposites based MSCs.

Sample	Current density (A/g)	C_s (Fg^{-1})	E ($Whkg^{-1}$)	P (Wkg^{-1})
GO	2.5	314	42	2.4
$CoFe_2O_4$@GO	2.5	389	53	1
$CoFe_2O_4$/PEDOT	2.5	315	43	0.9
$CoFe_2O_4$@GO/PEDOT	2.5	435	62	0.9
$CoFe_2O_4$@GO/PEDOT	5	398	54	1.5
$CoFe_2O_4$@GO/PEDOT	10	365	49	3.2

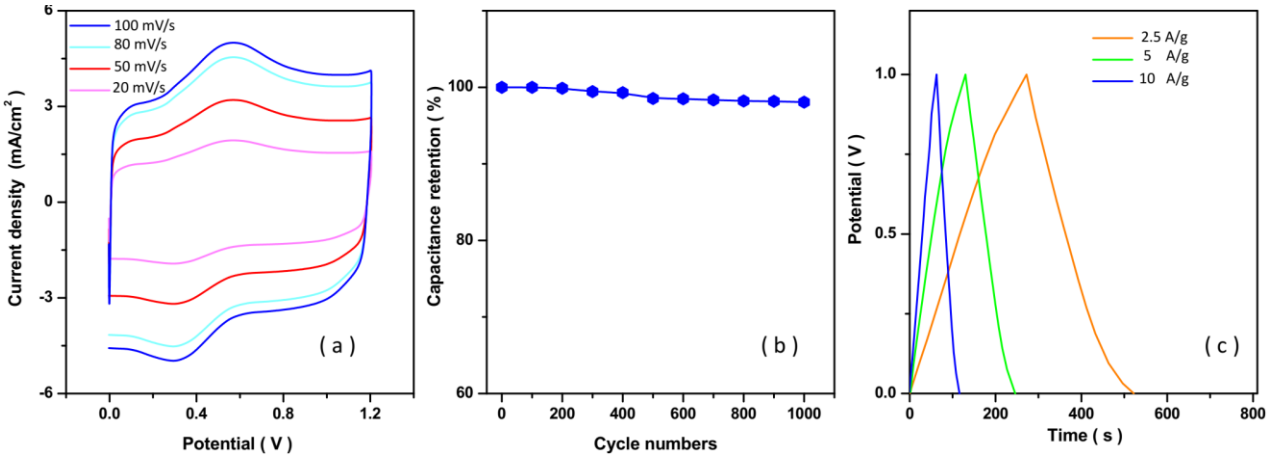

Figure 4. (a) CV at different scan rates from 20 to 100 mV/s, (b) GCD curves at current densities from 2.5 to 10 A/g of $CoFe_2O_4$@GO/PEDOT in potential range from 0 to 1.2 V and (c) capacitance retention with respect to cycle numbers for $CoFe_2O_4$@GO/PEDOT.

Figure 4a indicates that the rectangular-like CV curve of $CoFe_2O_4$@GO/PEDOT displays an increase in loop area with an increase in the scan rate from 5 to 100mV/s, demonstrating the increase in the current response and stability of CoFe2O4@GO/PEDOT nanocomposite-based MSCs. Further

studies were conducted on the rate capability of the $CoFe_2O_4$@GO/PEDOT electrode through measurements of the GCD curves at current densities of 2.5, 5, and 10 A/g. Figure 4b depicts the resultant GCD profiles of the $CoFe_2O_4$@GO/PEDOT electrode which are symmetric, signifying excellent reversible charging-discharging performance. The obtained values for C_s, E and P of $CoFe_2O_4$@GO/PEDOT nanocomposite based MSC at current densities of 2.5, 5, and 10 A/g are presented in Table 1. It is observed that $CoFe_2O_4$@GO/PEDOT demonstrates excellent rate capability and high specific capacitance retention even at very high current densities. It exhibits specific capacitances of 398 and 365 Fg^{-1} with 92% and 83% capacitance retention with increase the current density from 5 to 10 A/g, indicating the capacitance decreases with increasing current density because the diffusion and transfer of ions are limited at higher current densities [61, 62].

Table 3. Comparison between these results for $CoFe_2O_4$@GO/PEDOT nanocomposite based MSC and reported MSCs.

Electrode material	**Supporting electrolyte**	**C_s (F/g)**	**E (Wh/kg)**	**P (W/kg)**	**Current density (A/g)**	**Ref**
Amorphous nickel hydroxide nanospheres	1 M KOH	153	35.7	490	4.3	[63]
N/P co-doped ordered mesoporous carbon	6 M KOH	392	20.2	225	1	[64]
nitrogen-doped active carbon/graphene	6 M KOH	378.9	13.1	12.5	2	[65]
coffee grounds-derived/1T Reduced GO	1 M H_2SO_4	440	153.8	8750	0.5	[66]
MoS_2/C	1 M Na_2SO_4	201.4	--	--	0.2	[67]
Activated microwave exfoliated GO	1-butyl-3-methyl-imidazolium Tetrafluoroborate/acetonitrile	166	70	250	5.7	[68]
Porous Activated Reduced GO	1 M tetraethylammonium tetrafluoroborate/ acetonitrile	120	26	500	10	[69]
Activated microwave exfoliated GO	1-ethyl-3-methylimidazolium bis-(trifluorosulfonyl)imide/ acetonitrile	174	74	338	4.2	[70]
PEDOT:PSS/CoFe2O4 / Carbon Fiber Cloth	1 M Na_2SO_4	426	25.17	620.7	1	[71]
rGO/$CoFe_2O_4$/PEDOT: PSS	1 M KOH	0.0345	25.9	135.3	0.001	[72]
$CoFe_2O_4$@GO/PEDOT	100 g/l PVA/H2SO4	435	62	0.9	2.5	This work
		398	54	1.5	5	
		365	48	3.2	10	

Figure 4c shows the results of the study on the cycling stability of $CoFe_2O_4$@GO/PEDOT nanocomposite based MSC as another important parameter of MSC. The cycling stability of the

sample was evaluated over 1000 continuous charge-discharge cycles at a scan rate of 50mV/s at room temperature. It can be found that the highly porous $CoFe_2O_4$@GO/PEDOT electrode displays outstanding capacitance retention of about 96% after 1000 cycles. There is a small decrease in specific capacitance after 500 cycles (~3 %). This decrease may be related to dissociation of the bimetal oxide ions during the redox process [73]. After 500 cycles, there is no significant change in specific capacitance value, demonstrating the good cycling stability of $CoFe_2O_4$@GO/PEDOT nanocomposite based MSCs.

Table 3 shows the comparison between these results for $CoFe_2O_4$@GO/PEDOT nanocomposite based MSC and reported MSCs. It can be observed that the developed nanocomposite-based MSC in this study shows better or comparable performance than other reported MSCs which can be attributed to synergetic effect of $CoFe_2O_4$@GO composite and porous conductive polymer PEDOT which provides good electrical conductivity and large surface area [71, 72].

4. CONCLUSION

This study focused on the fabrication of $CoFe_2O_4$@GO/PEDOT as stretchable nanocomposite based MSCs and studies of its structural and electrical properties and electrochemical characterization for MSCs applications. The hydrothermal method was used for the preparation of $CoFe_2O_4$@GO/PEDOT. Structural studies demonstrated the successful synthesis of $CoFe_2O_4$@GO/PEDOT, and synergistic effects of $CoFe_2O_4$ nanoparticles, GO nanosheets and coral-like morphology of PEDOT enhanced the effective surface area and provided the high porosity surface. Results of the study of the electrical properties of samples showed that the GO had the higher conductivity value, and electrical conductivity was decreased with the addition of $CoFe_2O_4$ and PEDOT to the GO-based nanocomposite. $CoFe_2O_4$ also showed the lower conductivity. Results of electrochemical studies indicated that the areal specific capacitance, energy density and power density of CoFe2O4@GO/PEDOT nanocomposites based MSCs were obtained at 435F/g, 62Wh/kg and 0.9W/kg, respectively, at a current density of 2.5A/g in electrolyte of 100g/l PVA/H_2SO_4. A comparison between the results for $CoFe_2O_4$@GO/PEDOT nanocomposite based MSC and reported MSCs showed the better or comparable performance than other reported MSCs. In the study, the cycling stability of developed MSC showed an outstanding capacitance retention of about 96% after 1000 cycles, demonstrating the good cycling stability of $CoFe_2O_4$@GO/PEDOT nanocomposite based MSCs.

ACKNOWLEDGMENTS
The research was supported by the National Natural Science Foundation of China: Theoretical study on quantum states generation and quantum information process with optical cavity system 11447149.

References

1. W. Liu, Y. Zheng, Z. Wang, Z. Wang, J. Yang, M. Chen, M. Qi, S. Ur Rehman, P.P. Shum and L. Zhu, *Advanced Materials Interfaces*, 8 (2021) 2001978.

2. L. Jiang, Y. Wang, X. Wang, F. Ning, S. Wen, Y. Zhou, S. Chen, A. Betts, S. Jerrams and F.-L. Zhou, *Composites Part A: Applied Science and Manufacturing*, 147 (2021) 106461.
3. F. Li, Y. Li, J. Qu, J. Wang, V.K. Bandari, F. Zhu and O.G. Schmidt, *Nano Materials Science*, 3 (2021) 154.
4. C. Shen, S. Xu, Y. Xie, M. Sanghadasa, X. Wang and L. Lin, *Journal of Microelectromechanical Systems*, 26 (2017) 949.
5. Z. Zhang, L. Feng, H. Liu, L. Wang, S. Wang and Z. Tang, *Inorganic Chemistry Frontiers*, 9 (2022) 35.
6. M. Khosravi, *Journal of Eating Disorders*, 8 (2020) 1.
7. Z. Lv, Y. Luo, Y. Tang, J. Wei, Z. Zhu, X. Zhou, W. Li, Y. Zeng, W. Zhang and Y. Zhang, *Advanced Materials*, 30 (2018) 1704531.
8. D.G. Mackanic, T.-H. Chang, Z. Huang, Y. Cui and Z. Bao, *Chemical Society Reviews*, 49 (2020) 4466.
9. Y. Li, D.D. Macdonald, J. Yang, J. Qiu and S. Wang, *Corrosion Science*, 163 (2020) 108280.
10. L. Liu, H. Zhao and Y. Lei, *InfoMat*, 1 (2019) 74.
11. M. Beidaghi and Y. Gogotsi, *Energy & Environmental Science*, 7 (2014) 867.
12. T. Sang Tran, N.K. Dutta and N. Roy Choudhury, *Materials*, 12 (2019) 978.
13. G. Luo, Q. Zhang, M. Li, K. Chen, W. Zhou, Y. Luo, Z. Li, L. Wang, L. Zhao and K.S. Teh, *Nanotechnology*, 32 (2021) 405402.
14. B. Ji, F. Zhang, X. Song and Y. Tang, *Advanced materials*, 29 (2017) 1700519.
15. X. Zhang, Y. Tang, F. Zhang and C.S. Lee, *Advanced Energy Materials*, 6 (2016) 1502588.
16. C. Guo, C. Ye, Y. Ding and P. Wang, *IEEE Transactions on Power Delivery*, 36 (2020) 2374.
17. H. Fu, B. Gao, C. Hu, Z. Liu, L. Hu, J. Kan, Z. Feng and P. Xing, *Nanotechnology*, 33 (2021) 075703.
18. L. Guo, C. Ye, Y. Ding and P. Wang, *IEEE Transactions on Power Delivery*, 36 (2020) 3231.
19. L. Li, Y. Shan, F. Wang, X. Chen, Y. Zhao, D. Zhou, H. Wang and W. Cui, *ACS Applied Materials & Interfaces*, 13 (2021) 48525.
20. M. Khosravi, *Current Psychology*, 40 (2021) 5735.
21. M. Shaterian, A. Aghaei, M. Koohi, M. Teymouri and A. Mohammadi-Ganjgah, *Polyhedron*, 182 (2020) 114479.
22. H.R. Kim, J.H. Lee, S.K. Lee, Y. Chun, H.Y. Yoo, H.U. Lee, H.S. Kwak, C. Park, J.H. Lee and S.W. Kim, *Journal of Energy Storage*, 44 (2021) 103458.
23. Y. Wang, Y. Ma, G. Guo, Y. Zhou, Y. Zhang, Y. Sun and Y. Liu, *International Journal of Electrochemical Science*, 12 (2017) 2135.
24. T. Fan, C. Huang, R. Chen, J. Xu, C. Wang and Y. Qian, *International Journal of Electrochemical Science*, 12 (2017) 7659.
25. J. Li, J. Guo, X. Zhang, Y. Huang and L. Guo, *International Journal of Electrochemical Science*, 12 (2017) 1157.
26. R. Zhang, W. Zhang, M. Shi, H. Li, L. Ma and H. Niu, *Dyes and Pigments*, (2021) 109968.
27. N. Gurbani, C.-P. Han, K. Marumoto, R.-S. Liu, R.J. Choudhary and N. Chouhan, *ACS Applied Energy Materials*, 1 (2018) 5907.
28. N. Kasapoğlu, A. Baykal, Y. Köseoğlu and M. Toprak, *Scripta Materialia*, 57 (2007) 441.
29. R. Rezapour-Nasrabad, *Electronic Journal of General Medicine*, 15 (2018) em73.
30. L. Zhang, R. Jamal, Q. Zhao, M. Wang and T. Abdiryim, *Nanoscale Research Letters*, 10 (2015) 148.
31. H.U. Lee, J.-H. Jin and S.W. Kim, *Journal of industrial and engineering chemistry*, 71 (2019) 184.
32. H. Maleh, M. Alizadeh, F. Karimi, M. Baghayeri, L. Fu, J. Rouhi, C. Karaman, O. Karaman and R. Boukherroub, *Chemosphere*, (2021) 132928.

33. Y. Orooji, B. Tanhaei, A. Ayati, S.H. Tabrizi, M. Alizadeh, F.F. Bamoharram, F. Karimi, S. Salmanpour, J. Rouhi and S. Afshar, *Chemosphere*, 281 (2021) 130795.
34. H.-S. Jeong, H. Kim, K.-I. Jo, J. Jang, J.-H. Choi and J. Koo, *Applied Surface Science*, 508 (2020) 144416.
35. Z. Savari, S. Soltanian, A. Noorbakhsh, A. Salimi, M. Najafi and P. Servati, *Sensors and Actuators B: Chemical*, 176 (2013) 335.
36. C. Sumathi, P. Muthukumaran, P. Thivya, J. Wilson and G. Ravi, *RSC Advances*, 6 (2016) 81500.
37. N. Derakhshan, D. Derakhshan, A. Derakhshan, G. Hashemi, M. Fallahzadeh, M. Basiratnia, Z. Bazargani, H. Jalaeian and S. Malek-Hosseini, *Saudi Journal of Kidney Diseases and Transplantation*, 22 (2011) 339.
38. K.-H. Müller, G. Wei, B. Raguse and J. Myers, *Physical Review B*, 68 (2003) 155407.
39. M. Motevasselian, S.S. Gargari, S. Younesi, P. Pooransari, P. Saadati, M. Mirzamoradi, S. Savad, M.M.T. Amin, M.-H. Modarresi and M. Afrakhteh, *Molecular cytogenetics*, 13 (2020) 1.
40. S.-L. Shi, L.-Z. Zhang and J.-S. Li, *Journal of polymer research*, 16 (2009) 395.
41. M. Bakhtiyari, M. Mirzamoradi, P. Kimyaiee, A. Aghaie, M.A. Mansournia, S. Ashrafi-Vand and F.S. Sarfjoo, *Fertility and sterility*, 104 (2015) 649.
42. A. Daraghmeh, S. Hussain, I. Saadeddin, L. Servera, E. Xuriguera, A. Cornet and A. Cirera, *Nanoscale research letters*, 12 (2017) 1.
43. G. Liu, J. Shao, Y. Gao, Z. Chen and Q. Qu, *Chinese Journal of Chemistry*, 35 (2017) 67.
44. Y. Tian, C. Yang, W. Que, X. Liu, X. Yin and L.B. Kong, *Journal of Power Sources*, 359 (2017) 332.
45. M. Mirzamoradi, F. Hasani Nejhad, R. Jamali, Z. Heidar and M. Bakhtiyari, *The Journal of Maternal-Fetal & Neonatal Medicine*, 33 (2020) 2533.
46. W. Choi, H.-C. Shin, J.M. Kim, J.-Y. Choi and W.-S. Yoon, *J. Electrochem. Sci. Technol*, 11 (2020) 1.
47. J. Lin and X. Du, *Micromachines*, 12 (2021) 1195.
48. X. Deng, J. Li, S. Zhu, F. He, C. He, E. Liu, C. Shi, Q. Li and N. Zhao, *Journal of Alloys and Compounds*, 693 (2017) 16.
49. R. Li, X. Dong, C. He, Z. Liu, L. Huang and Y. Yang, *International Journal of Electrochemical Science*, 12 (2017) 144.
50. G. Jiang and S. Xie, *International Journal of Electrochemical Science*, 14 (2019) 5422.
51. P. Tang, L. Han and L. Zhang, *ACS applied materials & interfaces*, 6 (2014) 10506.
52. A. Elschner and W. Lövenich, *MRS bulletin*, 36 (2011) 794.
53. A.M. Teli, S.A. Beknalkar, S.A. Pawar, D.P. Dubal, T.D. Dongale, D.S. Patil, P.S. Patil and J.C. Shin, *Energies*, 13 (2020) 6124.
54. S.M.M. Dezfouli and S. Khosravi, *European Journal of Translational Myology*, 30 (2020) 8712.
55. K. Gholami Laelabadi, R. Moradian and I. Manouchehri, *ACS Applied Energy Materials*, 3 (2020) 5301.
56. J. Ma, S. Zheng, Y. Cao, Y. Zhu, P. Das, H. Wang, Y. Liu, J. Wang, L. Chi and S. Liu, *Advanced Energy Materials*, 11 (2021) 2100746.
57. A. Bahrami, A. Nateghian, S. Salehi, G. Bahoush, S. Talebi, S. Ghasemi, S. Razi and N. Rezaei, *Acta Medica Iranica*, 58 (2020) 38.
58. Z. Peng, J. Lin, R. Ye, E.L. Samuel and J.M. Tour, *ACS applied materials & interfaces*, 7 (2015) 3414.
59. R. Savari, H. Savaloni, S. Abbasi and F. Placido, *Sensors and Actuators B: Chemical*, 266 (2018) 620.

60. F. Chahshouri, H. Savaloni, E. Khani and R. Savari, *Journal of Micromechanics and Microengineering*, 30 (2020) 075001.
61. B. Cheng, R. Cheng, F. Tan, X. Liu, J. Huo and G. Yue, *Nanoscale research letters*, 14 (2019) 1.
62. S. Salehi, M. Kamali and M. Radgoodarzi, *Progress in Pediatric Cardiology*, 62 (2021) 101378.
63. H. Li, M. Yu, F. Wang, P. Liu, Y. Liang, J. Xiao, C. Wang, Y. Tong and G. Yang, *Nature communications*, 4 (2013) 1.
64. X. Xin, H. Kang, J. Feng, L. Sui, H. Dong, P. Zhao, B. Pang, Y. Chen, Q. Sun and S. Ma, *Chemical Engineering Journal*, 393 (2020) 124710.
65. Q. Xie, R. Bao, A. Zheng, Y. Zhang, S. Wu, C. Xie and P. Zhao, *ACS Sustainable Chemistry & Engineering*, 4 (2016) 1422.
66. J.-H. Choi, C. Lee, S. Cho, G.D. Moon, B.-s. kim, H. Chang and H.D. Jang, *Carbon*, 132 (2018) 16.
67. L.-Q. Fan, G.-J. Liu, C.-Y. Zhang, J.-H. Wu and Y.-L. Wei, *International Journal of Hydrogen Energy*, 40 (2015) 10150.
68. Y. Zhu, S. Murali, M.D. Stoller, K. Ganesh, W. Cai, P.J. Ferreira, A. Pirkle, R.M. Wallace, K.A. Cychosz and M. Thommes, *science*, 332 (2011) 1537.
69. L.L. Zhang, X. Zhao, M.D. Stoller, Y. Zhu, H. Ji, S. Murali, Y. Wu, S. Perales, B. Clevenger and R.S. Ruoff, *Nano letters*, 12 (2012) 1806.
70. T. Kim, G. Jung, S. Yoo, K.S. Suh and R.S. Ruoff, *ACS nano*, 7 (2013) 6899.
71. K. Song, X. Wang, J. Wang, B. Zhang and R. Yang, *ChemistrySelect*, 4 (2019) 1685.
72. J. Song, W. Li, J. Xin, W. Wang, K. Song, X. Chen and G. Yin, *Applied Surface Science*, 568 (2021) 150915.
73. P.-C. Chen, G. Shen, S. Sukcharoenchoke and C. Zhou, *Applied Physics Letters*, 94 (2009) 043113.